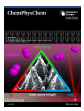

From Femtosecond to Nanosecond Laser Microstructuring of Conical Aluminum Surfaces by Reactive Gas Assisted Laser Ablation

Simon Rauh,[a] Karl Wöbbeking,[a] Mingji Li,[a] Wolfgang Schade,[a, b] and Eike G. Hübner*[a, c]

A conical microstructure is one of the most versatile surface textures obtained by ultrashort laser micromachining. Besides an increased surface area, unique surface properties such as superhydrophilicity, increased absorptivity; and thermal emissivity can be tailored. On metals, usually ultrashort laser pulses in the femtosecond to low picosecond range are used to obtain these surface structures, whereas nanosecond laser pulses favor melting processes. Herein, we report on an investigation of reactive gas atmospheres such as oxygen, steam, and halogens during laser micromachining of aluminum with 6 ns laser pulses. At a reduced pressure of 20 hPa (air) with additional iodine vapor as reactive species, we found a perfectly microconical structured surface to be formed with nanosecond laser pulses. The resulting surface structures were proven to be free of residual halogens. The application of nanosecond instead of femtosecond laser pulses for the surface structuring process allows to apply significantly less complex laser sources.

1. Introduction

Femtosecond (fs) laser microstructuring is a versatile technology to target the surface structure and surface properties of various materials ranging from metals to semiconductors and ceramics. Recent reviews summarize the range of substrates, achievable surface structures and applications of the laser structured surfaces.[1–3] A special focus is given to the microconical surface structure, often denoted as columnar structures, spikes, nanowhiskers, and bumps, which is referred to "the most common microstructure" in femtosecond laser processing.[2] These structures provide a large increase in the specific surface area, the cones can act as light traps, surface adhesion can be adjusted precisely and various more surface properties can be optimized.[4–8] On aluminum, femtosecond laser structuring is challenging due to its low melting point (see Table 1) and high thermal conductivity.[9] Nevertheless, homogeneously microconically structured surfaces of aluminum have been reported in literature.[10–15] The resulting surfaces provide the expected unique properties strongly differing from the plane metal. Characteristic features of the microconical aluminum surfaces include controlled light absorbance[13,14] and targeted wettability/adhesion[15] properties (superhydrophobic aluminum). Figure 1a visualizes a microconically structured

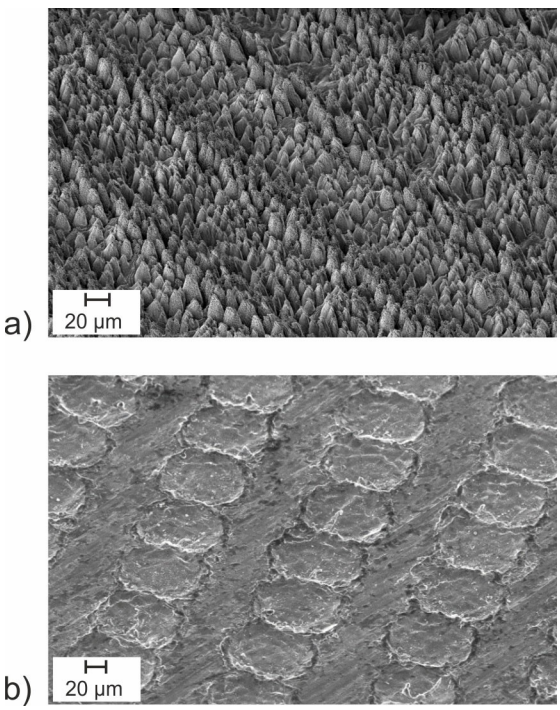

Figure 1. SEM images of aluminum surfaces treated with laser pulses. a) Femtosecond laser pulses ($\lambda = 800$ nm, $\tau = 60$ fs, $J = 2.61$ J cm^{-2}, $N = 250$, $f = 10$ kHz, $S_{spot} = 100$ µm, $D_{line} = 100$ µm, N_2 atmosphere). b) Single nanosecond laser pulses ($\lambda = 1064$ nm, $\tau = 2$ ns, $J = 12.73$ J cm^{-2}, $S_{spot} = 100$ µm, air).

[a] S. Rauh, K. Wöbbeking, M. Li, Prof. Dr. W. Schade, Prof. Dr. E. G. Hübner
Fraunhofer Heinrich Hertz Institute HHI, Fiber Optical Sensor Systems, Am Stollen 19 H, 38640 Goslar, Germany
E-mail: eike.huebner@tu-clausthal.de
[b] Prof. Dr. W. Schade
Clausthal University of Technology, Institute of Energy Research and Physical Technologies, Am Stollen 19 B, 38640 Goslar, Germany
[c] Prof. Dr. E. G. Hübner
Clausthal University of Technology, Institute of Organic Chemistry, Leibnizstr. 6, 38678 Clausthal-Zellerfeld, Germany

Supporting information for this article is available on the WWW under https://doi.org/10.1002/cphc.202000418

Table 1. Physical properties of aluminum, the reagents and reaction products discussed here.

	m.p.[33] [°C]	b.p.[33] [°C]	Vapor pressure[33] [hPa] at 25 °C	Electronegativity[33]
Al	660	2519	–	1.6
Al_2O_3	2053	~2975	–	–
O_2	−219	−183	>1013	3.4
H_2O	0	100	32 199 (60 °C); 474 (80 °C)	–
I_2	114	184	0.3[34] 0.16 (18 °C); 1.0 (40 °C)	2.7
AlI_3	188	382	<0.0007[35]	

aluminum surface obtained by femtosecond laser ablation with 60 fs laser pulses.

In contrast to femtosecond laser microstructuring, nanosecond (ns) laser pulses generally lead to other mechanisms of material ablation and surface structuring.[16–18] Material ablation is combined with melting processes and the resulting structure is dominated by molten and resolidified material.[18] This effect is visualized in Figure 1b, which represents a series of single pulses with a pulse width of 2 ns on an aluminum surface. The molten aluminum solidifies around the crater of each laser shot. Still, there is a strong motivation for nanosecond laser structuring. In general, ns laser systems are much more stable and cost-effective in comparison to fs laser setups.[19] Consequently, various examples in literature describe nanosecond laser structured aluminum surfaces.[20–25] In all these examples, melting processes during the surface structuring process are clearly visible in scanning electron microscopic (SEM) or laser scanning microscopic (LSM) images. It must be noted that regular columnar surface structures have been achieved by ns laser structuring, yet the column distance is larger by one order of magnitude in comparison to the irregular microconical surface obtained by fs laser structuring. This is explained by different mechanisms leading to the microcolumns. The origin of the columns is based on crossings of molten grooves in case of ns laser structuring in contrast to the self-organized microstructures formed during femtosecond laser ablation.[10,21]

Besides the physical parameters, the surrounding gas atmosphere during laser irradiation significantly affects the structuring process. Reactive gases can lead to additional etching processes on the surface. For example, on silicon and steel an SF_6 atmosphere during the structuring process with femtosecond laser pulses has been reported to form deeper or sharper and finer structures.[4,10] Recently, we reported on a comparison of the microconical surface structure on titanium realized by near-picosecond (750 fs) pulses from a high-power laser setup in the presence of reactive gases to the surface obtained with the usual 60 fs pulses of Ti:sapphire laser.[26] C. H. Crouch, E. Mazur et al. demonstrated that silicon can be structured towards a coarser microconical surface with 30 ns pulses from a KrF^+ Excimer laser at 248 nm in the presence of SF_6.[5] The resulting cones are approx. 5 times larger than in case of the sample irradiated with fs laser pulses, but clearly based on self-organized processes.

Here, we investigated the surface structuring of aluminum with a robust Nd:YAG laser source with 6 ns laser pulses in the presence of various reactive gases. Since both aluminum as well as nanosecond laser pulses favor melting processes, a careful parameter selection has been performed. To the best of our knowledge, we report for the first time on a homogeneous microconical surface obtained on aluminum by self-organizing processes induced from nanosecond laser pulses.

2. Results and Discussion

The nanosecond laser source applied here is a robust Nd:YAG laser with a center wavelength at $\lambda = 1064$ nm, a pulse length of 6 ns, a maximal pulse energy of $E = 50$ mJ and a pulse repetition rate of $f = 20$ Hz. To investigate the ablation process in the presence of reactive gases (Figure 2a), all experiments have been performed within a stainless-steel chamber (Figure 2c) equipped with an NIR transparent glass window, temperature and pressure sensors, inlet and outlet valves and electric heating. First, the laser parameters have been optimized at air to obtain a homogeneously structured surface without grooves formed by the incident laser beam. The theory of laser ablation of aluminum with femtosecond and nanosecond laser pulses is well investigated in literature.[9–11,27–31] The ablation threshold for femtosecond pulses is given at $J = 0.4\ J\,cm^{-2}$ (180 fs at 775 nm).[9] The ablation threshold for 5 ns pulses at 1064 nm is given at a fluence of approx. $J = 5\ J\,cm^{-2}$,[28,30] which is roughly 10 times larger than the femtosecond ablation threshold and readily explained by the reduced peak power. A second threshold is reported above a fluence of $J = 15\text{-}30\ J\,cm^{-2}$ (for 5 ns pulses at 1064 nm), at which a sudden increase in ablation occurs due to phase explosion processes.[29,31] These processes lead to sharp pits in the center of the ablated region.[32] To achieve a homogeneous surface structure, these pits are undesired. Consequently, a laser fluence between these two thresholds has been chosen here. Parameter variation was started with a fluence of $J = 20.7\ J\,cm^{-2}$ at a pulse diameter of $S = 555\ \mu m$. The LSM image of a single crater with these parameters reveals the complete absence of deep pits and presents a homogeneously ablated region (see Figure S2 of the Supporting Information). Scanning the aluminum surface with these parameters and $N = 11$ pulses per spot at a line distance of $D = 400\ \mu m$ revealed isolated molten lines on the surface (see Figure S3). By reducing the line distance and increasing the spot size, the surface structure developed more and more homogeneously towards a porous and rough surface (see

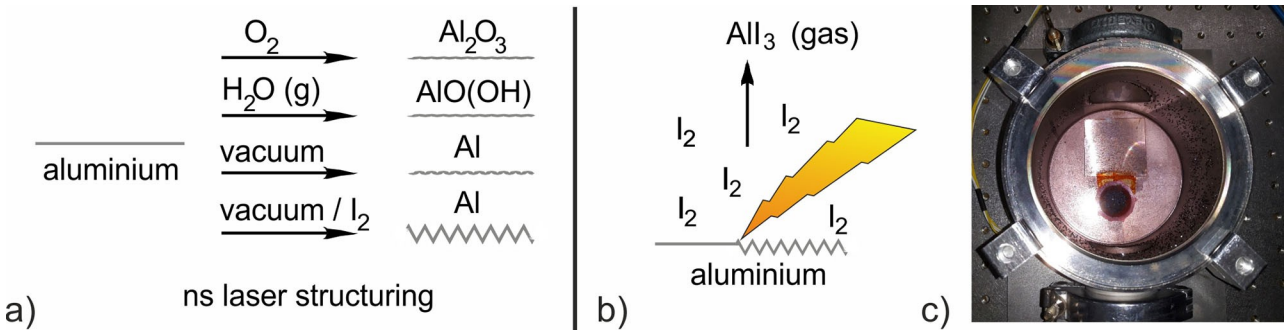

Figure 2. Sketch of nanosecond laser structuring a) in the presence of reactive gases and resulting surface chemistry, b) processed in the presence of iodine and formation of low boiling aluminum triiodide, and c) photographic image of the processing chamber with iodine vapor at a total pressure of 20 hPa at 40 °C.

Figures S3–S7 for selected examples). The final laser parameters with a fluence of $J = 9.80$ Jcm^{-2}, a spot diameter of $S = 806$ µm, a number of pulses per spot of $N = 16$ and a line distance of $D = 25$ µm led to aluminum samples with a dark grey surface appearance. The SEM image (Figure 3b) reveals the microstructure, which differs significantly from the sharp grooves typically achieved in ns laser structuring, which is explained by the large spot diameter, comparably low fluence and strongly overlapping lines. The structured aluminum sample provides a significantly increased surface roughness compared to the plane surface (see Table 2 for all surface properties), yet the surface is not strongly structured and not comparable to the microconical surface of **Al-ref** obtained with fs laser pulses (Figure 1a). The chemical surface composition determined by energy-dispersive X-ray spectroscopy (EDX) reveals a significant amount of 48 atom-% of oxygen, indicating an aluminum oxide layer formed during laser processing at air. The dull appearance of the surface is confirmed by reflective UV/Vis spectroscopy, which reveals an absorptivity of roughly 84% (at 600 nm). "Black metals" are a common feature obtained by femtosecond

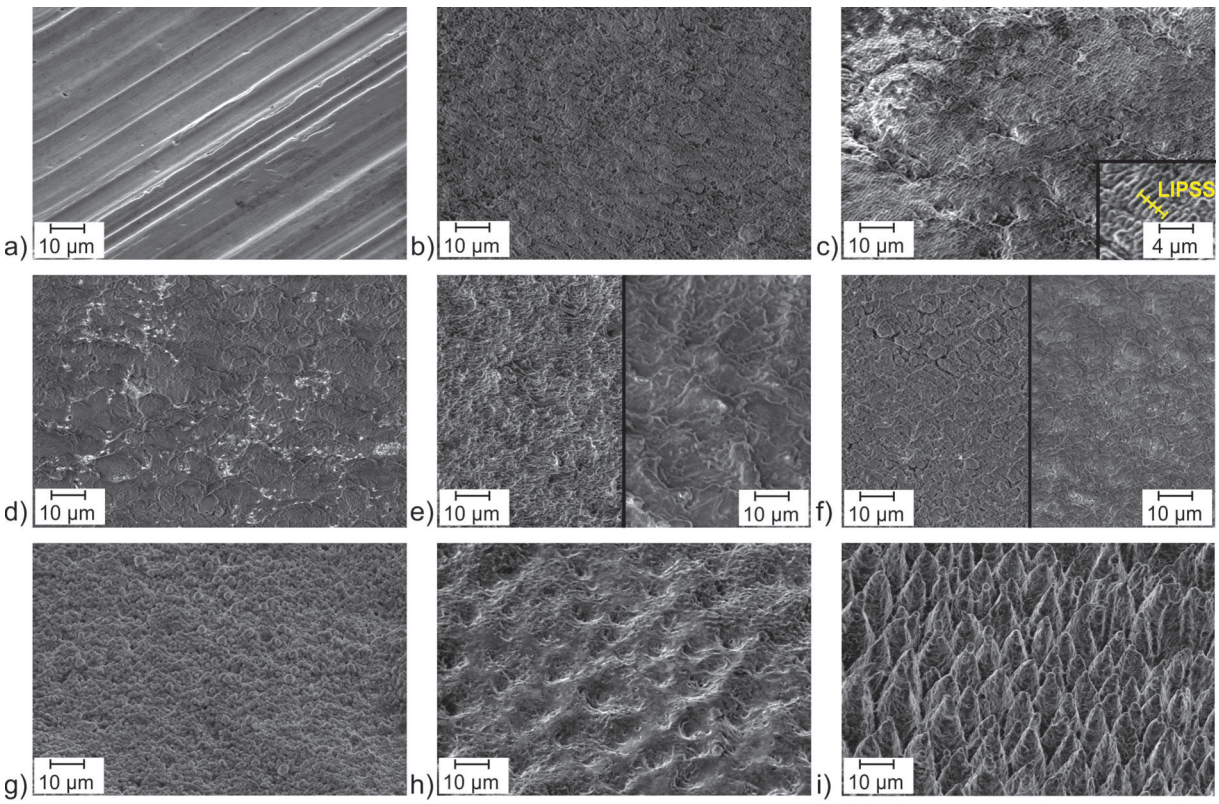

Figure 3. SEM images of aluminum samples: a) untreated surface, b)–i) laser structured with nanosecond laser pulses at (b) air, (c) nitrogen, (d) oxygen, (e) water (l) at 25 °C (left) and 60 °C (right), (f) water vapor at 60 °C (left) and 80 °C (right), (g) iodine/air (1013 hPa), (h) vacuum (20 hPa), and (i) iodine/vacuum (20 hPa). Laser parameters: $\lambda = 1064$ nm, $\tau = 6$ ns, $J = 9.80$ J cm^{-2}, $S_{spot} = 806$ µm, $N = 16$, $D_{line} = 25$ µm for all samples except (c): $S_{spot} = 718$ µm, $D_{line} = 75$ µm.

Table 2. Properties of the aluminum surfaces treated with 6 ns laser pulses in various atmospheres.

Sample	Atmosphere (at 25 °C)	Surface composition [atom-%] O	I	Θ[a] [°]	ε[b] [%]	α[c] [%]	R_a[d] [μm]	Surf. enlargement factor[d]
Al	untreated	7.1 ± 0.3	–	63 ± 3	9 ± 2	36	0.40 ± 0.05	1
Al-ref[e]	N_2	2.7 ± 0.4	–	→180	39 ± 2	77	4.4 ± 0.9	7
Al-air	air	48.0 ± 3.9	–	118 ± 3	30 ± 3	84	1.8 ± 0.1	2
Al–N_2	N_2	43.7 ± 3.6	–	131 ± 3	36 ± 8	–	1.5 ± 0.1	2
Al–O_2	O_2	57.7 ± 4.7	–	→0	83 ± 6	88	1.9 ± 0.5	2
Al–H_2O(l)	water	10.4 ± 0.8	–	109 ± 3	10 ± 2	–	1.3 ± 0.2	2
Al–H_2O(g)	steam (60 °C)	63.9 ± 3.1	–	→0	53 ± 11	90	0.7 ± 0.1	2
Al–I_2	air + I_2	33.0 ± 2.6	0.02 ± 0.03	138 ± 3	17 ± 3	–	0.8 ± 0.2	2
Al-vac	20-30 hPa	15.0 ± 1.1	–	129 ± 3	9 ± 1	–	1.1 ± 0.1	2
Al-vac-I_2	20-30 hPa + I_2	1.9 ± 0.3	0.02 ± 0.04	→180	25 ± 6	56	4.8 ± 0.8	9

[a] Contact angle, measured with water 1 week after laser structuring. [b] Thermal emissivity, at 100 °C. [c] Absorptivity, at 600 nm. [d] Surface roughness and enlargement factor, measured by LSM. [e] processed with a Ti:sapphire laser setup and 60 fs pulses under N_2 atmosphere for comparison (see Figure 1a).

laser processing.[13,14] In contrast, the reference sample **Al-ref** obtained with fs pulses provides an absorptivity of only 77 %. This is readily explained by the surface composition, which reveals **Al-ref** to consist of 91 % pure aluminum and consequently reflecting significant amounts of light. Repeating the femtosecond laser structuring process in the presence of air leads to a deep black aluminum surface (see Figure S15) but with a less pronounced surface structure covered with a porous oxide layer (see Figure S11). The deep black color can be explained by a combination of structural parameters (light trap) and the chemical surface composition here. Oxygen-deficient aluminum oxide reveals a dark color[36] and consequently the combination of a structured surface and the aluminum-rich oxide layer leads to the black appearance. This assumption matches with the absorptivity of 84 % obtained for the nanosecond laser processed sample, since the oxide layer leads to absorption processes, but the surface structure is not sufficient to support complete light absorption.

Surface structuring with nanosecond pulses has been repeated in a nitrogen atmosphere to determine the influence of oxidation processes. The resulting surface (see Figure S10) is less homogeneous than in the presence of oxygen and surface structuring processes are visibly reduced. The chemical surface composition reveals a surprisingly high amount of oxygen of 44 atom-% (in contrast to 3 atom-% oxygen for the sample processed with femtosecond laser pulses under a nitrogen atmosphere). Since during ns laser processing the hot, molten aluminum surface is exposed to the nitrogen atmosphere, partial formation of aluminum nitride (AlN) can be assumed. AlN decomposes upon contact with wet air and aqueous cleaning of the samples to aluminum hydroxide, which can explain the resulting oxygen content. As an interesting aspect, the typical periodic parallel lines induced by laser irradiation (laser induced periodic surface structures, LIPSS[37]) have been detected with a periodicity of approx. 1 μm in the sample. The effect is more pronounced by laser processing with an increased line distance of 75 μm and is visualized in Figure 3c. These LIPSS have not been detected for any sample in the presence of reactive gases at any parameter set during this work and visualize the domination of etching processes in the presence of additional reactants.

Switching to pure oxygen at 1013 hPa as first reactive species and applying the given parameter set for nanosecond laser structuring revealed a slightly coarser surface structure (Figure 3d). The chemical composition shows an oxygen content of 58 atom-% O, which matches nicely with the formation of aluminum oxide (Al_2O_3, 60 atom-% O). The surface appearance is dark grey, again readily explained by the slight oxygen deficiency and formation of dark aluminum oxide.[36] The absorptivity of the surface is uniformly around $\alpha = 90\,\%$ across the visible spectrum (see Figure 4e). The water contact angle of the sample processed in an oxygen atmosphere indicated superhydrophilicity (Table 2). In general, contact angles of laser processed surfaces must be discussed with caution, since freshly prepared surfaces are usually superhydrophilic while they switch to superhydrophobic after some days. Reasons for the change of the contact angle are condensation reactions of terminal hydroxide groups on the metal surface (M–OH) towards metaloxane bridges and a surface coverage with organic impurities.[21,38,39] Here, contact angles have been documented one week after laser processing. The superhydrophilicity of the sample **Al–O_2** is in clear contrast to the bare aluminum surface or the surface obtained after laser processing at air or the fs laser processed sample, respectively. The superhydrophilicity is in accordance with the chemical analysis and can be explained by a porous oxide layer.

The thermal emissivity of the samples has been measured at 100 °C by MIR imaging as an additional surface property, which can be tailored by femtosecond laser treatment.[2] The sample structured in presence of oxygen reveals a strong increase in emissivity from $\varepsilon = 9\,\%$ (plain aluminum surface) to $\varepsilon = 83\,\%$ (see Figure 4d). Again, this effect can be explained by a combination of surface structuring and chemical composition. The emissivity of bulk alumina (Al_2O_3) is reported to approx. $\varepsilon = 80\,\%$ at 100 °C matching with this result.[40] In contrast, the oxide-free, but structured surface of the sample **Al-ref** processed with fs laser pulses reveals an emissivity of $\varepsilon = 39\,\%$. Overall, the oxygen atmosphere changes the surface chemistry towards an oxide layer but does not significantly assist in the

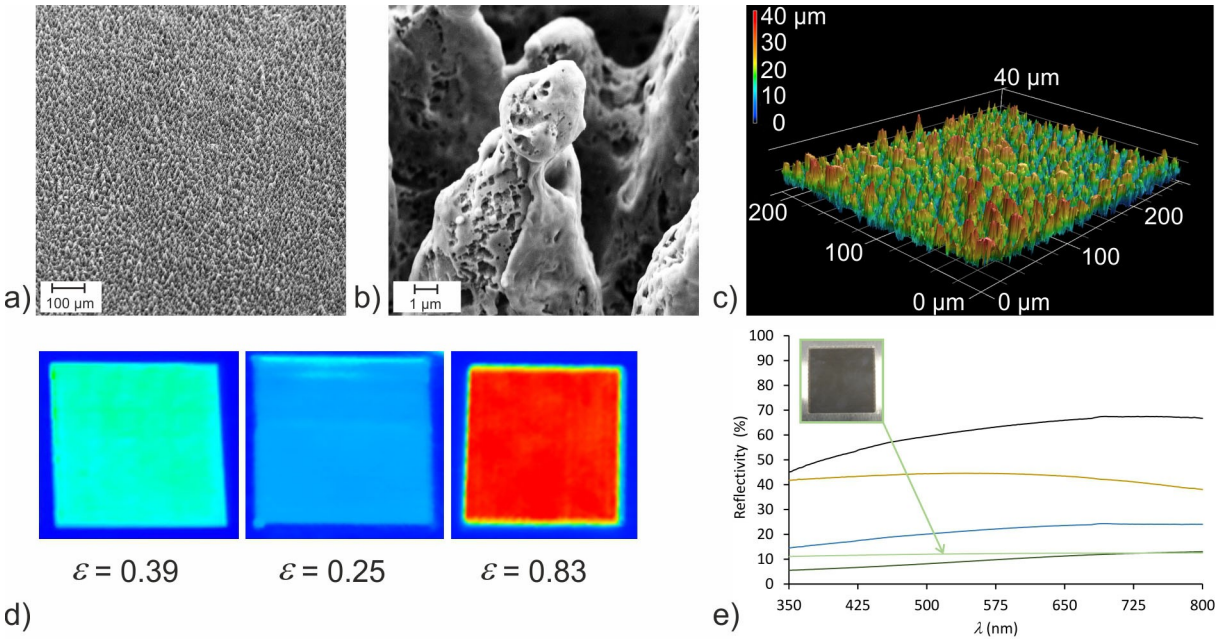

Figure 4. a) SEM image of a large surface area from the sample **Al-vac-I_2** treated with 6 ns pulses at 20 hPa in the presence of iodine, b) close-up view of a single microcone, c) depth information of **Al-vac-I_2** obtained from LSM, d) thermal emissivity MIR images at 100 °C for the sample processed with femtosecond laser pulses **Al-ref** (left), processed with 6 ns pulses at 20 hPa in the presence of iodine (**Al-vac-I_2**, middle) and with 6 ns pulses in the presence of oxygen (**Al–O_2**, right), and e) UV/Vis reflectance spectra (black: untreated Al, blue: **Al-ref**, beige: **Al-vac-I_2**, green: **Al–O_2** and dark green **Al–H_2O(g)** (processed with 6 ns pulses in water vapor at 60 °C).

structuring process. This may be explained by the high boiling point of aluminum oxide (Table 1). Oxides formed during ns laser irradiation do not evaporate from the surface.

Since aluminum is known to be attacked by water, surface structuring was repeated in liquid phase and the aluminum plate was immersed 1 cm below the water surface. Laser structuring of aluminum in liquid-confined environment has been investigated in literature and generally proceeds well.[41,42] Explosive water evaporation and shock compression have been given as reasons for an increased ablation rate. With the standard parameter set here, a homogeneous surface covered with resolidified melt in form of a wavy structure has been obtained (Figure 3e, left). Obviously, melting processes have dominated surface structuring in this case. The chemical surface composition is in accordance with the absence of chemical reactions and presents basically an aluminum surface. Consequently, the contact angle of $\Theta = 109°$ is in agreement with a structured aluminum surface and the emissivity matches with pure aluminum, too. The ns laser structuring process has been repeated with water at a temperature of 60 °C (Figure 3e, right). Basically the same observations have been made. The surface structure is significantly coarser and larger amounts of material are molten towards larger solidified structures, yet etching processes are absent. Overall, water was found to be too unreactive to assist in material ablation.

Since cooling processes seemed to dominate in liquid water, hot water vapor was applied as reactive medium in contrast to liquid water. The vapor pressure of water was adjusted by the chamber temperature to 200 hPa (60 °C) and 470 hPa (80 °C), respectively (Table 1). The SEM images reveal a surface structure close to the structure achieved at air and at oxygen (Figure 3f). The chemical composition of the sample **Al–H_2O(g)** obtained at 60 °C is in clear contrast to the surface obtained in liquid phase confinement and reveals an oxygen content of 64 atom-%. This value is above the theoretical maximum for alumina (Al_2O_3, 60 atom-% O). Consequently the formation of aluminum hydroxide [$Al(OH)_3$, 75 atom-% O (excluding H, invisible in EDX)] and alumina monohydrate (AlO(OH), 66 atom-% O) can be assumed. Initially, the formation of $Al(OH)_3$ is to be expected upon reaction of Al with water. At elevated temperatures, stepwise condensation of aluminum hydroxide to alumina monohydrate and alumina takes place.[43] The EDX analysis matches quite well with slightly oxygen-deficient AlO(OH), which is in agreement with the dark black surface color (absorptivity around $\alpha = 90\%$) again. The thermal emissivity is rather low at $\varepsilon = 53\%$ and the MIR image at 100 °C reveals a significant inhomogeneity (see Figure S13) although the surface structure is visibly and according to SEM completely homogeneous. Consequently, we assume a mixture of the aluminum hydroxides to be formed at the conditions of the ns laser surface treatment in a water vapor atmosphere. Switching to water vapor at 80 °C and increasing the vapor pressure to 470 hPa did not significantly change the structuring process (Figure 3f, right).

Since the formation of high-boiling oxides inhibited deeper structuring processes in all the cases discussed above, halogens had been applied as additive to ns laser structuring. The concept is presented in Figure 2b. Halogens react readily with

aluminum, can etch the surface and the resulting aluminum halides provide low boiling points. Consequently, the surface is not protected by an oxide layer any longer. First, bromine was investigated as additive at ambient conditions. Bromine assists in the laser structuring of titanium surfaces with picosecond laser pulses.[26] Unfortunately, the reactivity of bromine towards aluminum is too high and together with a comparably high bromine concentration caused by the vapor pressure of 250 hPa (see Table 1), the aluminum surface was massively attacked by bromine before laser irradiation was performed (see Figure S12 of the supplementary material). Consequently, iodine was applied as least reactive halogen. The processing chamber saturated with iodine vapor reveals an intense violet appearance (see Figure 2c), but at the wavelength of the incident laser beam at 1064 nm iodine is completely NIR transparent[26] and absorption processes can be disregarded. Owed to the low vapor pressure of iodine of 0.3 hPa at 25 °C, the total amount of iodine inside the chamber is low. The chamber with a volume of 0.65 L provides approx. 0.01 mmol iodine. Assuming an ablation of a layer of 10 μm aluminum (see below) would require a stoichiometric amount of 0.15 mmol iodine per 1 cm^2 (see Figure 2b). Consequently, an iodine reservoir with excess iodine was kept inside the chamber during laser processing to keep the iodine concentration constant. At ambient pressure with additional iodine in air, the ns laser processed structure did not significantly differ from ns laser structuring at pure air (compare Figure 3b and 3 g). The grainy structure appears slightly more pronounced and deeper although this is not confirmed by the surface roughness. As an interesting aspect, the elemental composition reveals a significantly reduced amount of oxygen of 33 atom-% O for the sample processed in the presence of iodine (**Al–I_2**) in comparison to the sample processed at air (48 atom-% O). This observation has been confirmed by the reduced emissivity of $\varepsilon = 17\,\%$ and proves the general concept of halogens as additive to reduce surface protection from an oxide layer to be applicable. Fortunately, residual iodine was not detected on the surface (see Table 2).

Since the fraction of iodine in comparison to oxygen was too low to significantly affect the structuring process, ns laser structuring was repeated at a reduced pressure. Surface structuring of aluminum with nanosecond laser pulses at a reduced pressure has been investigated in literature.[44] The ablation depth is significantly increased by a factor of two for the fluence of 10 J cm^{-2} applied here at high vacuum and at 13 hPa in an inert gas atmosphere in comparison to 1013 hPa at air.[44] With the standard parameter set applied here at 20 hPa, a pronounced surface structure has been observed (Figure 3h). The surface is covered by broad, flat but regular bumps. Looking at the structure more closely reveals fine pores, which may be formed by boiling aluminum. The boiling point of aluminum is reached during ns laser processing, for example up to a depth of 3 μm in the material with 10 ns pulses.[45] Unlike our observations for femtosecond laser processing in vacuum,[26] the glass window of the processing chamber remained clean during ns laser processing at 20 hPa and laser structuring of larger surfaces is achieved without problems. As expected, the chemical composition of the surface processed at the reduced pressure reveals a low amount of 15 atom-% O and the emissivity of $\varepsilon = 9\,\%$ does not differ from the bare aluminum surface. The contact angle of $\Theta = 129°$ reveals hydrophobicity, which is in accordance with a basically oxide-free, but structured surface.

Repeating the ns laser treatment with the same parameter set at a pressure of 20 hPa, but in the presence of iodine (0.3 hPa at 25 °C) revealed a strong impact on the surface structuring process. The combination of etching processes and the formation of low boiling AlI_3 (see Table 1) led to a surface coverage with well-defined microcones (Figure 3i). The cones are clearly not formed at distinct spots on the surface such as crossings of laser-structured lines, but by self-organizing processes. The tip of the cones reveals as a sharp spike, which can be seen as a further indication for etching processes. The chemical surface composition reveals an amount of only 2 atom-% of oxygen. These findings back the expected mechanism of material ablation by aluminum iodide formation and evaporation. The surface consists basically of pure aluminum (92 atom-% Al) comparable to the fs processed sample **Al-ref** (91 atom-% Al). Consequently, the reflectivity ($\alpha = 56\,\%$) is still rather high, despite the conical structure motif. This is in accordance with the sample **Al-ref** as discussed above. The surface of **Al-vac-I_2** was proven to be iodine-free (Table 2). Fortunately, the application of iodine to assist the laser structuring process does not lead to a contamination of the surfaces with halides. In accordance with the absence of aluminum oxide, the thermal emissivity of $\varepsilon = 25\,\%$ is rather low (see Figure 4d), which is in consistence with the fs laser processed sample. In accordance with the SEM images, the surface roughness of the sample is significantly increased in comparison to all other ns laser processed samples discussed here. The arithmetic average of the roughness R_a is determined to 4.8 μm, which is comparable to the reference sample ($R_a =$ 4.4 μm). The height of the microcones has been analyzed by LSM (Figure 4c). and reveals an average height of 10–15 μm for each tip, which is in good accordance with fs laser processed microconical surfaces. The pillar density has been calculated to 0.01 cones μm^{-2}, which matches with the range of self-organized microconical surfaces obtained by femtosecond laser micromachining.[5,46] The surface enlargement factor, i.e. the surface area compared to the plane surface, is calculated to 9, which demonstrates the pronounced surface structure. It must be noted, that BET measurements usually reveal a larger surface area, which can be explained by a porosity not recognized by the LSM.[47] Figure 4a visualizes the homogeneity of the microconical structure on larger areas. We found samples of 2×2 cm^2 to be processed without any problems. Due to the low vapor pressure of iodine, the amount of halogen consumed during the laser structuring process of the large sample is around 100 milligrams. Looking at the microcones more in detail by high-resolution SEM (Figure 4b) visualizes porous substructures of the cones, possibly caused by etching processes, and reveals some molten areas on the sub-micrometer scale. Overall, the cones provide a very well-defined and bare appearance, which matches with the chemical composition.

The formation of the cones has been investigated more in detail. From a chemical point of view, the iodine concentration within the chamber has been varied. Since the vapor pressure of iodine shows a strong dependence on the temperature around 25 °C, the partial pressure of iodine was halved from 0.3 hPa to 0.16 hPa by reducing the temperature from 25 °C to 18 °C. The SEM images (see Figure S8) demonstrate, that sufficient etching is not observed any longer and the cones are not isolated, but partly connected to a larger structure. Increasing the temperature to 40 °C (v.p.(I_2) = 1 hPa) leads to strong etching and deep channels formed on the surface, but melting processes start to dominate the structure building process (see Figure S8).

From a physical point of view, structure formation can be discussed looking at the edge of the structured area. According to the scanning speed of the pulsed laser beam, each spot on the surface is hit by a train of $N = 16$ pulses. Since a large laser spot diameter of approx. 800 μm has been applied and the lines on the sample have been scanned with a line distance of $D =$ 25 μm during ns laser processing, the number of laser pulses on each spot on the surface summarize to $16 \times 32 = 512$ pulses per spot if these additional pulse trains are taken into account. At the upper and lower border of the structured area, a boundary zone with a diameter of 400 μm exists, in which the number of pulses on each spot increases from 16 pulses to 512 pulses by 16 pulses every 25 μm. Figure 5 visualizes this peripheral zone of the structure and indeed it takes the full 400 μm until the microconical structure is achieved, which then is homogeneously covering the surface. Starting at the plane surface (bottom left), first slight etching processes, then channel formation and finally the microcones evolving from the channels are visible. With different parameter sets applied at the same ambient conditions, e.g. increasing the line distance to $D = 50$ μm or increasing the scanning speed and consequently reducing the number of pulses of each pulse train to $N = 8$, conical structure formation is absent. Consequently, we can assume that 512 laser pulses are necessary to form the microconical structure. Interestingly, these findings match well with the observations documented in literature for microconical surface formation by femtosecond laser irradiation.[10,48] First, ripples are formed and an increasing number of pulses per spot leads to microgrooves and initial microconical structures, followed by intensifying of the structure and finally large pillar formation with a height of 10 μm if the number of pulses reaches 120–300.[10,48]

Directly contrasting the femtosecond laser processed sample **Al-ref** and the sample **Al-vac-I_2** processed with nanosecond laser pulses in a iodine atmosphere at 20 hPa visualizes the similarity of the structures (Figure 6). The homogeneous dull appearance on a macroscopic scale (Figure 6a) as well as the conical structure of the same dimension on a microscopic scale (Figure 6b) appear similar. Together with an identical chemical surface composition, the surface properties match with each other. The water contact angle of both structures reaches superhydrophobicity (Figure 6c). The superhydrophic surface is readily explained by water droplets positioned on top of the columnar structures with air filling the gap between the cones.[48]

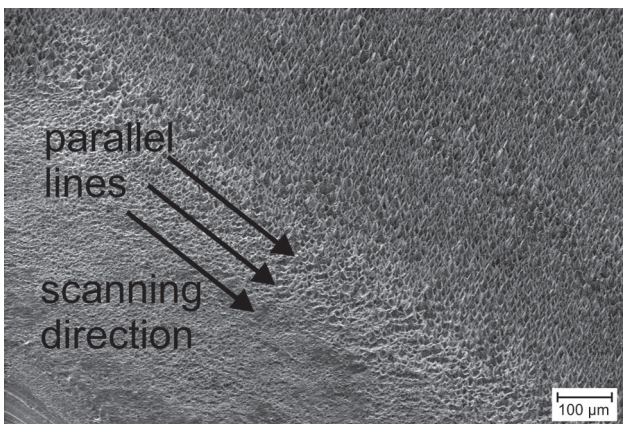

Figure 5. Development of the surface structure beginning at the edge of the ns laser processed area on the plane aluminum plate (bottom left) towards the homogeneous microconical surface (top right) with increasing number of overlapping laser processed lines.

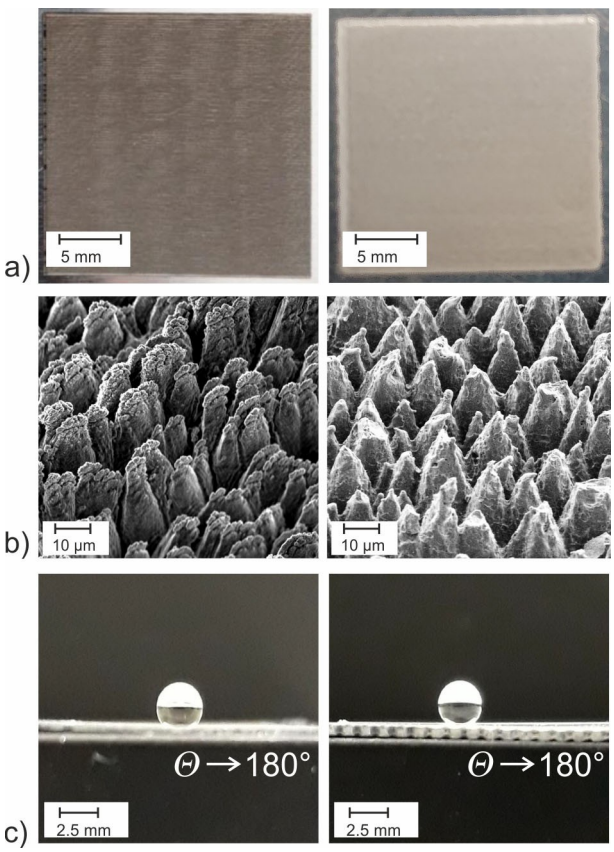

Figure 6. Aluminum surface treated with 60 fs laser pulses in a nitrogen atmosphere (Al-ref, left) and 6 ns laser pulses in an iodine/air atmosphere at 20 hPa (Al-vac-I_2, right). a) Photographic image, b) SEM image, and c) water contact angle.

3. Conclusions

Femtosecond laser microstructuring allows to achieve unique surface structures and surface properties by self-organizing processes. In contrast, nanosecond laser structuring favors melting processes and surface structures are frequently not obtained by self-organizing processes, but macroscopically designed by the path laser beam. As a consequence, the resulting structures are dominated by molten and resolidified material und usually larger by one order of magnitude.

The addition of reactive gases to initiate etching processes on the laser-processed area can be applied in laser microstructuring to achieve sharper and deeper structures. Here, we investigated the addition of reactive gases to the structuring process of aluminum with 6 ns laser pulses. Due to its low melting point, molten structures are strongly favored on aluminum. In an oxygen and water vapor atmosphere, the surface was found to be covered by oxide and hydroxide layers, while etching processes were inhibited. In contrast, the addition of iodine at a reduced total pressure of 20 hPa strongly increased etching and structure formation on the aluminum surface. At a comparable weak laser fluence of 10 $J\,cm^{-2}$, a homogeneous surface structure covered with microcones was achieved by self-organizing processes. The height and density of the microcones is comparable to the structure obtained by femtosecond laser micromachining. Consequently, the chemical and physical surface properties showed up to be nearly identical, too.

The moderate vacuum conditions of 20 hPa and the low vapor pressure of iodine lead to a convenient process handling. Minimal amounts of iodine are sufficient to saturate the atmosphere within the chamber. Larger surfaces could be processed without impairing the quality of the microstructure. Upcoming work focuses on an extension towards further materials and the integration of high-power fiber lasers to speed-up the process.

Experimental Section

Plates of aluminum (99.5 + %) with 0.8 mm thickness (rapa GmbH) have been cleaned by ultrasonication with acetone and deionized water. All chemicals have been obtained from Sigma Aldrich unless stated differently. Iodine, bromine, oxygen (Linde), nitrogen (Linde) and sodium thiosulfate have been used as received. Reflective UV/Vis Spectra have been recorded with a Jasco V650 spectrophotometer equipped with an integrating sphere (Jasco ISV-722). Diffuse reflectance spectra are referenced to a standard white sample (reflectivity $\rho = 100\,\%$) from Jasco. Absorptivity values α have been calculated according to $\alpha + \rho = 1$. Emissivity measurements have been taken at 100 °C with a Testo T885 MIR camera. Contact angles have been measured from photographic images with water droplets of a volume of 10 µL on the samples. Contact angles have been measured 30 s after application of the drop and 1 week after laser processing of the sample. Scanning electron microscopy (SEM) images have been taken with an EVO MA10 (Zeiss) SEM operated at 10 kV. Elemental composition of surfaces has been determined with an energy dispersive X-ray spectroscopy (EDX) unit (Bruker XFlash 6/30) integrated in the SEM at 10 kV with a penetration depth resulting from the voltage of the electron beam of approx. 1 µm in aluminum. High resolution SEM images have been taken with a Zeiss DSM 982 Gemini microscope with field emission cathode. A laser scanning microscope (LSM) operated at 408 nm (Keyence VK-X200) has been used for microscopic depth information and the determination of surface roughness.

Our general setup for laser surface processing with femtosecond pulses has been described previously.[49] Here, a Nd:YAG nanosecond laser source (Big Sky Ultra) with a centre wavelength of $\lambda =$ 1064 nm and a pulse length of $\tau = 6$ ns has been integrated in the setup. Spot diameters are given at the threshold width of $1/e^2$. Besides the preliminary parameter variation, the following parameters have been applied for all final samples at reactive gas atmospheres. A spot diameter of approximately $S = 806$ µm on the surface has been adjusted by a 420 mm f-theta objective. The average optical laser output power of $P = 1$ W leads to a pulse energy of $E = 50$ mJ and a laser fluence of $J = 9.80\,J\,cm^{-2}$ at a repetition rate of $f = 20$ Hz. The scanning speed of $v = 0.001$ m/s of the laser beam on the surface results in every spot on the surface to be hit by a number of $N = 16$ laser pulses. Areas of $5 \times 5\,mm^2$ (parameter variation) and $2 \times 2\,cm^2$ (final samples) have been irradiated in lines with a line distance of $D = 25$ µm. All experiments have been performed within an air-tight stainless-steel processing chamber (inner diameter 10 cm) equipped with a borosilicate window, temperature and vacuum sensors and 2 inlet and outlet valves positioned on an 800 W heating plate. The total volume of the chamber is 0.65 L. The inner atmosphere of the chamber has been exchanged by repeated evacuation and flushing with oxygen or nitrogen, equilibrated with the vapor pressure of bromine or iodine at ambient pressure or in vacuo for 1 h or with water vapor at the desired temperature. All samples have been cleaned by ultrasonication in deionized water for 5 min. Samples have been stored at ambient conditions. The processing chamber has been rinsed with sodium thiosulfate solution after all experiments with halogens.

For comparison, samples have been processed with a Ti:sapphire laser source with $t = 60$ fs laser pulses at a wavelength of 800 nm according to a setup reported previously.[47] Samples treated with $\tau = 2$ ns pulses from a fiber laser at ambient air have been obtained from Trotec.

Acknowledgements

We sincerely thank Peggy Knospe (Clausthal University of Technology, Institute of Particle Technology) for high resolution SEM images, Thomas Gimpel (Clausthal University of Technology, Research Center for Energy Storage Technologies, EST) for help with the femtosecond laser setup and Trotec Laser GmbH for fiber-laser structured aluminum plates. Open access funding enabled and organized by Projekt DEAL.

Conflict of Interest

The authors declare no conflict of interest.

Keywords: aluminum · femtosecond · laser structuring · nanosecond · surfaces

[1] A. Y. Vorobyev, C. Guo, *Laser Photonics Rev.* **2013**, *7*, 385–407.
[2] K. M. T. Ahmmed, C. Grambow, A.-M. Kietzig, *Micromachines* **2014**, *5*, 1219–1253.
[3] K. Sugioka, Y. Cheng, *Light Sci. Appl.* **2014**, *3*, e149.
[4] R. Younkin, J. E. Carey, E. Mazur, J. A. Levinson, C. M. Friend, *J. Appl. Phys.* **2003**, *93*, 2626–2629.
[5] C. H. Crouch, J. E. Carey, J. M. Warrender, M. J. Aziz, E. Mazur, F. Y. Génin, *Appl. Phys. Lett.* **2004**, *84*, 1850–1852.
[6] J. Heitz, C. Plamadeala, M. Muck, O. Armbruster, W. Baumgartner, A. Weth, C. Steinwender, H. Blessberger, J. Kellermair, S. V. Kirner, J. Krüger, J. Bonse, A. S. Guntner, A. W. Hassel, *Appl. Phys. A* **2017**, *123*, 734.
[7] E. Fadeeva, V. K. Truong, M. Stiesch, B. N. Chichkov, R. J. Crawford, J. Wang, E. P. Ivanova, *Langmuir* **2011**, *27*, 3012–3019.
[8] J. Yang, Y. Yang, B. Zhao, Y. Wang, X. Zhu, *Appl. Phys. B* **2012**, *106*, 349–355.
[9] W. Perrie, M. Gill, G. Robinson, P. Fox, W. O'Neill, *Appl. Surf. Sci.* **2004**, *230*, 50–59.
[10] B. K. Nayak, M. C. Gupta, *Opt. Lasers Eng.* **2010**, *48*, 940–949.
[11] G. M. Robinson, M. J. Jackson, *J. Mater. Eng. Perform.* **2006**, *15*, 155–160.
[12] S. Bashir, M. S. Rafique, W. Husinsky, *Radiat. Eff. Defects Solids* **2013**, *168*, 902–911.
[13] A. Y. Vorobyev, C. Guo, *Proc. SPIE-Int. Soc. Opt. Eng.* **2008**, *7005*, 1T1-1T8.
[14] N. Singh, D. R. Alexander, J. Schiffern, D. Doerr, *J. Laser Appl.* **2006**, *18*, 242–244.
[15] Y. Song, C. Wang, X. Dong, K. Yin, F. Zhang, Z. Xie, D. Chu, J. Duan, *Opt. Laser Technol.* **2018**, *102*, 25–31.
[16] A. Semerok, C. Chaléard, V. Detalle, S. Kocon, J.-L. Lacour, P. Mauchien, P. Meynadier, C. Nouvellon, P. Palianov, M. Perdrix, G. Petite, B. Sallé, *Proc. SPIE-Int. Soc. Opt. Eng.* **1998**, *3343*, 1049–1055.
[17] R. Le Harzic, N. Huot, E. Audouard, C. Jonin, P. Laporte, S. Valette, A. Fraczkiewicz, R. Fortunier, *Appl. Phys. Lett.* **2002**, *80*, 3886–3888.
[18] K.-H. Leitz, B. Redlingshöfer, Y. Reg, A. Otto, M. Schmidt, *Phys. Procedia* **2011**, *12*, 230–238.
[19] *Communications: Laser Technik Journal* **2015**, *12*, 22–26. DOI: 10.1002/latj.201590031.
[20] R. Jagdheesh, J. J. García-Ballesteros, J. L. Ocaña, Proceedings of Lasers in Manufacturing Conference – LiM 2015.
[21] Z. Yang, X. Liu, Y. Tian, *J. Colloid Interface Sci.* **2019**, *533*, 268–277.
[22] J. Zhao, J. Guo, P. Shrotriya, Y. Wang, Y. Han, Y. Dong, S. Yang, *Opt. Laser Technol.* **2019**, *117*, 134–141.
[23] R. Jagdheesh, J. J. García-Ballesteros, J. L. Ocaña, *Appl. Surf. Sci.* **2016**, *374*, 2–11.
[24] J. T. Cardoso, A. Garcia-Girón, J. M. Romano, D. Huerta-Murillo, R. Jagdheesh, M. Walker, S. S. Dimov, J. L. Ocaña, *RSC Adv.* **2017**, *7*, 39617–39627.
[25] J. Guo, X. Ma, X. Si, Z. Yang, J. Zhao, *IOP Conf. Ser.: Mater. Sci. Eng.* **2019**, *538*, 012021.
[26] K. Wöbbeking, M. Li, E. G. Hübner, W. Schade, *RSC Adv.* **2019**, *9*, 37598–37607.
[27] Y. Ito, I. Oguro, Y. Fukuzawa, S. Nakamura, *Proc. SPIE-Int. Soc. Opt. Eng.* **2000**, *4065*, 461–469.
[28] C. Porneala, D. A. Willis, *Appl. Phys. Lett.* **2006**, *89*, 211121.
[29] M. Stafe, I. Vlădoiu, C. Negutu, I. M. Popescu, *Rom. Rep. Phys.* **2008**, *60*, 789–796.
[30] A. H. A. Lutey, *J. Appl. Phys.* **2013**, *114*, 083108.
[31] M. Stafe, I. Vladoiu, I. M. Popescu, *Cent. Eur. J. Phys.* **2008**, *6*, 327–331.
[32] J. M. Fishburn, R. P. Mildren, D. Kapitan, M. J. Withford, D. J. W. Brown, J. A. Piper, *Proc. SPIE-Int. Soc. Opt. Eng.* **2000**, 3885, 453–460.
[33] *CRC Handbook of Chemistry and Physics*, 84th edition (Ed.: D. R. Lide), CRC Press LLC, Boca Raton **2004**.
[34] G. P. Baxter, C. H. Hickey, W. C. Holmes, *J. Am. Chem. Soc.* **1907**, *29*, 127–136.
[35] B. Brunetti, V. Piacente, P. Scardala, *J. Chem. Eng. Data* **2010**, *55*, 2164–2168.
[36] P. Nayar, A. Khanna, D. Kabiraj, S. R. Abhilash, B. D. Beake, Y. Losset, B. Chen, *Thin Solid Films* **2014**, *568*, 19–24.
[37] N. G. Zubrilin, I. V. Blonskiy, I. M. Dmitruk, O. E. Dombrovskiy, N. I. Berezovska, V. I. Stiopkin, *Semicond. Phys. Quantum Electron. Optoelectron.* **2017**, *20*, 48–54.
[38] J. Lu, T. Huang, Z. Liu, X. Zhang, R. Xiao, *Appl. Surf. Sci.* **2018**, *459*, 257–262.
[39] L. T. Zhuravlev, *Colloids Surf. A* **2000**, *173*, 1–38.
[40] M. E. Whitson in *Handbook of the infrared optical properties of Al2O3, carbon, MgO, and ZrO2, Vol. 1* (Ed.: M. E. Whitson), National Technical Information Service, Springfield **1975**, pp. I-10 - I-21.
[41] H. W. Kang, H. Lee, A. J. Welch, *J. Appl. Phys.* **2008**, *103*, 083101.
[42] Y. Cao, X. Zhao, Y. C. Shin, *J. Laser Appl.* **2013**, *25*, 032002.
[43] T. Sato, *Thermochim. Acta* **1985**, *88*, 69–84.
[44] A. M. Elsied, P. C. Dieffenbach, P. K. Diwakar, A. Hassanein, *Spectrochim. Acta Part B* **2018**, *143*, 26–31.
[45] S. T. Hendow, S. A. Shakir, *Opt. Express* **2010**, *18*, 10188–10199.
[46] B. K. Nayak, M. C. Gupta, K. W. Kolasinski, *Appl. Phys. A* **2008**, *90*, 399–402.
[47] A. Gabler, C. I. Müller, T. Rauscher, T. Gimpel, R. Hahn, M. Köhring, B. Kieback, L. Röntzsch, W. Schade, *Int. J. Hydrogen Energy* **2018**, *43*, 7216–7226.
[48] A. S. Alnaser, S. A. Khan, R. A. Ganeev, E. Stratakis, *Appl. Sci.* **2019**, *9*, 1554.
[49] S. B. Beil, T. Müller, S. B. Sillart, P. Franzmann, A. Bomm, M. Holtkamp, U. Karst, W. Schade, S. R. Waldvogel, *Angew. Chem.* **2018**, *130*, 2475–2479; *Angew. Chem. Int. Ed.* **2018**, *57*, 2450–2454.

Manuscript received: May 15, 2020
Revised manuscript received: June 18, 2020
Accepted manuscript online: June 19, 2020
Version of record online: July 10, 2020